Available online at www.sciencedirect.com
SCIENCE DIRECT®
Journal of Nuclear Materials 354 (2006) 36–48
journal of nuclear materials
www.elsevier.com/locate/jnucmat

First-principles study of alloying effect of transition metals on He in titanium ditritide

Y.X. Wu [a], R. Yang [a,1], H. Zheng [b], Y.M. Wang [a,*]

[a] Shenyang National Laboratory for Materials Science, Institute of Metal Research, Chinese Academy of Science, 72 Wenhua Road, Shenyang 110016, People's Republic of China
[b] Department of Special Environmental Materials, Institute of Metal Research, Chinese Academy of Science, 72 Wenhua Road, Shenyang 110016, People's Republic of China

Received 25 October 2005; accepted 2 February 2006

Abstract

Due to its inert reactivity with almost elements, ^{3}He produced from tritium decay has extremely detrimental effects on the tritide. To refrain from this ^{3}He-induced damage, an efficient way is to increase the stability of ^{3}He in metal tritide by alloying. Using a first-principles discrete variational method in two cluster models, one for a low ^{3}He concentration and the other for a high ^{3}He concentration, the authors study the alloying effect of 3d and 4d transition metals on the stability of ^{3}He in TiT_2 system. It is found that the preferring and metastable sites of ^{3}He are affected by ^{3}He concentration: ^{3}He prefers to stay at original tetrahedral interstitial site when ^{3}He concentration is low but moves to octahedral site when ^{3}He concentration is high enough. A criterion of alloying effect is proposed, according to which Nb, Y, Zr, Pd, Ru, Tc, Rh, Cr, Mo and Ag are suggested to be the beneficial alloying elements for increasing the stability of ^{3}He in the alloyed TiT_2 with a low ^{3}He concentration and Y, Nb, Mo, Zr, Cr, Tc, Ru, Rh and Cu for that with a high ^{3}He concentration. Our results of alloying effect are supported by the positron annihilation spectroscopy (PAS) measurements for He-implanted Ti, TiMoYAl and TiZrYAl films.

PACS: 21.60.Gx

1. Introduction

Tritium is an essential source used in nuclear industry, commonly stored in the form of a tritide or ditritide for the safety, easy recovery, and also much higher stored density than in its liquid form. The metals such as Pd, Ti, Sc, Er and U, and the intermetallic alloys such as $LaNi_5$, ZrCo, etc, are usually used for this purpose. In these metals and alloys, T decays with a half-life of circa 12.36 years [1,2] into a ^{3}He, an electron and an antineutrino. It is surprising that ^{3}He atoms produced from tritium decay do not immediately diffuse out of the lattice until some critical atomic ratio of ^{3}He/metal is reached [2,3] since ^{3}He is normally insoluble in

* Corresponding author. Tel.: +86 24 2397 1840; fax: +86 24 2389 1320.
E-mail address: ymwang@imr.ac.cn (Y.M. Wang).
[1] Present address: Department of Computer Science, Faculty of Engineer and Information Technology, Australian National University, Canberra, ACT 0200, Australia.

0022-3115/$ - see front matter © 2006 Elsevier B.V. All rights reserved.
doi:10.1016/j.jnucmat.2006.02.101

almost all tritides for its inert reactivity with other elements. To understand this phenomenon, there have been many experimental and theoretical studies [1–14] of ^{3}He in tritides, however, the states of ^{3}He atoms in metals and metal tritides are still in debate. Camp [2] and Weaver [4] believed the ^{3}He atoms are trapped at the octahedral interstitial sites in tritides with the fluorite crystal structure while Bowman and Attalla [10] suggested the ^{3}He atoms primarily reside in microscopic gas bubbles with dimensions <100 Å. To refrain from the damage caused by ^{3}He bubbles, Shaw et al. [8], Mansur et al. [12] and Goodhew et al. [13] proposed that by trapping ^{3}He in specific solutes, either the clustering of ^{3}He could be inhibited or a large quantity of very small ^{3}He clusters would be created to prevent the occurrence and consequently the outburst of large bubbles. The methods they suggested all include alloying of tritides. However, as far as we know, very limited information concerning alloying effects on the electronic structure of ^{3}He in tritides can be obtained.

Lots of studies confirm that cluster model can be used to simulate the crystal behavior if the number of the atoms in the cluster is sufficiently large. It is found that the behavior and electronic structure of H in clusters are similar to those in a crystal [15–18]. Besides quite a few reports about alloying effects on different systems by using the cluster model [19–25], Yang et al. [26] recently employed a cluster model to study the transition metal alloying effect on the chemical bonding in TiH_2. As a continuance of Yang's work [26], the goal of the present paper is to investigate the alloying effect of 3d and 4d transition metal elements on the behavior of ^{3}He in TiT_2.

2. Models and computational details

In this paper we used the discrete variational X_α (DV-X_α) method [27] based on density function theory (DFT) to investigate the alloying effect of transition metals on He in TiT_2. The exchange-correlation potential of Von Barth–Hedin [28] was adopted in the local density approximation (LDA) to DFT. The LDA has turned out to be much more successful than originally expected [29]. Although the generalized gradient approximation (GGA) has become widespread, it is generally found to improve the account of electron correlations in finite or semi-infinite systems, such as molecules and surfaces, but less helpful in infinite solids. In fact, Wolverton et al. [30] have given an evidence for it after carefully comparing LDA with GGA in their first-principle study of the structure properties of AlH_3, ScH_2, TiH_2, VH_2 and NiH. They found that typically LDA calculations of crystalline compounds underestimate lattice parameters with respect to experiment by circa 1–2% whereas GGA calculations may overestimate a similar amount, and the difference of formation energies between LDA and GGA is approximate to the zero-point energy (ZPE) correction for H_2, 0.25 eV/H_2, somewhat similar to our result, 0.268 eV/H_2. In our case of TiT_2 with T atom three times as heavy as H atom, the ZPE correction will be less important. And it was also pointed [30] that the formation energy difference between the two structures at same composition is independent of the ZPE for H_2, so that both LDA and GGA give almost same results. As mentioned below, the main concern in our calculations is just the binding energy difference between the two structures of He at different interstitial sites, therefore, LDA calculations seem to be reasonably accurate in our case.

The atomic orbitals in the present calculations were used including 1s, 2s, 2p, 3s, 3p, 3d, 4s, 4p for 3d transition elements (Sc, Ti, V, Cr, Mn, Fe, Co, Ni, Cu, Zn); 1s, 2s, 2p, 3s, 3p, 3d, 4s, 4p, 4d, 5s, 5p for 4d transition elements (Y, Zr, Nb, Mo, Tc, Ru, Rh, Pd, Ag, Cd); 1s for T(H) and ^{3}He (denoted as He below). The number of spatial integration points for these two models is 96 000 and 144 000, respectively. The binding energy E_b is defined as $E_b = E_{ref} - E_{total}$, where E_{total} is the total energy of a cluster and E_{ref} the sum of the energies of the free atoms composing the cluster. This definition means that the larger the E_b, the more stable the system is.

TiT_2 is of CaF_2-type crystal structure with the lattice constant of 4.40 Å [2], and tritons reside at the eight tetrahedral sites. Two models are proposed here to simulate the migration ability (or instability) of He leaving these tetrahedral sites and to explore the alloying effects of 3d and 4d transition metals on this migration ability for a low and a high He concentration, respectively. As shown in Fig. 1(a), model 1 is a 94-atom cluster with C3 symmetry, in which only one He atom occupies the tetrahedral site nearest to the center of the cluster, which is the octahedral site of the unit cell. Model 2 shown in Fig. 2 is a 143-atom cluster with Oh symmetry, containing eight He atoms at the tetrahedral sites nearest to the central metal atom. In these two models, the maximum and minimum dark spheres denote He

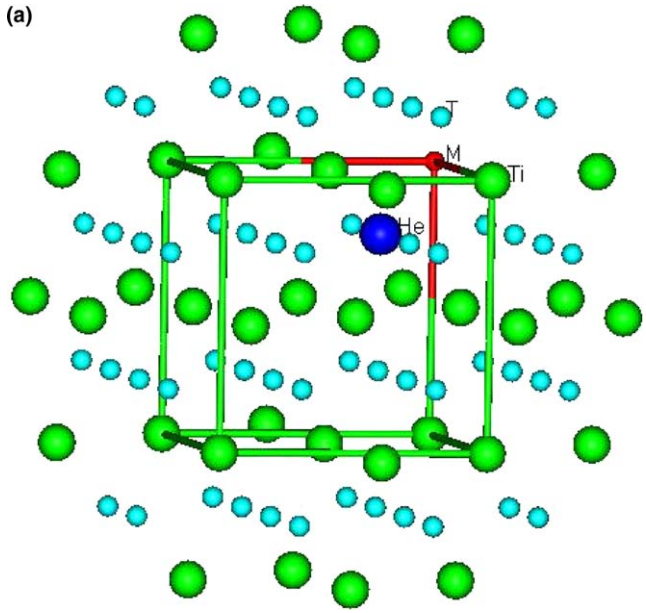

Fig. 1(a). Model 1 employed in the calculation for a low He concentration. The maximum and minimum dark spheres denote for He atom and alloying element M, respectively, and the maximum and minimum light spheres for Ti and T atoms, respectively. One unit cell of TiT_2 included in this cluster is indicated.

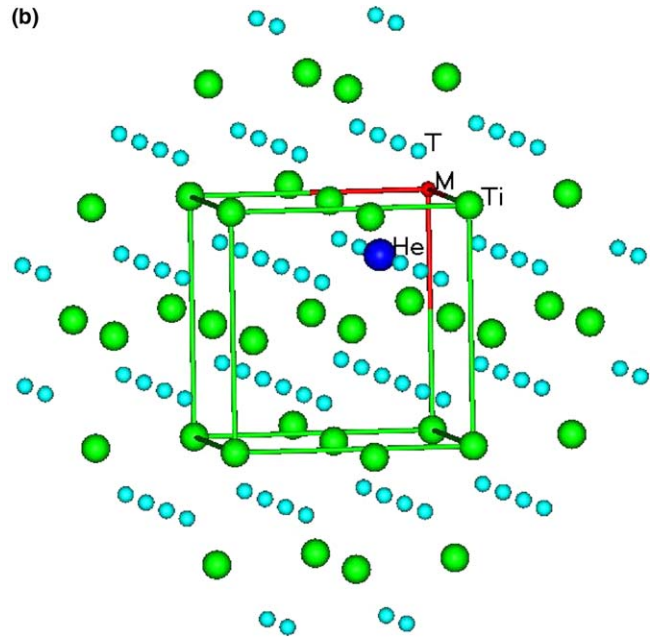

Fig. 1(b). The enlarged cluster of model 1 (shown in Fig. 1(a)) employed in the calculation for a low He concentration. The maximum and minimum dark (light) spheres have the same meaning as in Fig. 1(a).

atom and alloying element M (for unalloyed case M = Ti), respectively, and the maximum and minimum light spheres denote Ti and T atoms, respectively. Clearly, the He produced from the T decay occurs randomly in TiT_2, but for the sake of simplicity, we assume that the He-doped structure of TiT_2 at some point of aging time can be represented by model 1 or 2. Model 1 presents a configuration

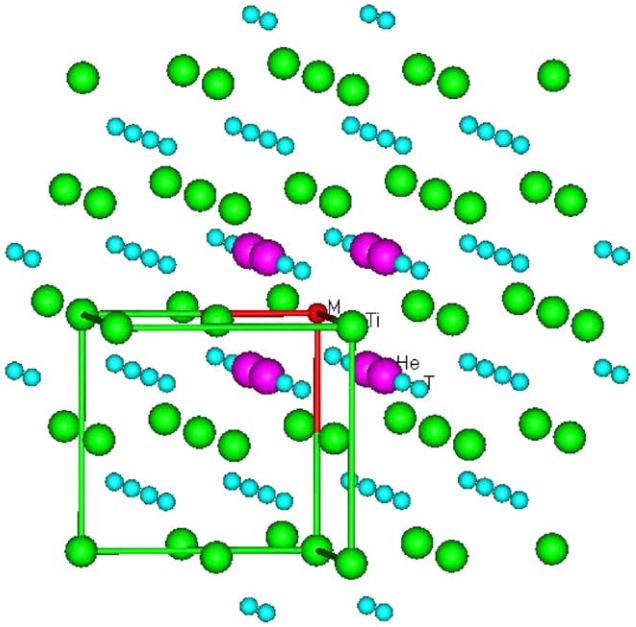

Fig. 2. Model 2 employed in the calculation for a high He concentration. The maximum and minimum dark (light) spheres have the same meaning as in Fig. 1(a). One incomplete unit cell of TiT_2 in this model is plotted.

occurring at the very beginning of aging time, with only one T decayed into He; and model 2 shows an imaginary initial He bubble-like configuration, which is not experimentally evidential nor necessarily inexistent. The atomic ratio of He to Ti is $1/38 \approx 2.63$ at.% in model 1 and $8/55 \approx 14.55$ at.% in model 2. According to the formula [7]

$$C_{\mathrm{He}} = C_{T,0}[1 - \exp(-\lambda t)], \tag{1}$$

where C_{He} is the He concentration, $C_{T,0}$ the initial T concentration, $\lambda = 1.774 \times 10^{-9}\mathrm{s}^{-1}$ the decay constant and t the aging time, we can find that these two models correspond to some structures of He-doped TiT_2 after circa 17 weeks and 89 weeks of aging time, respectively. Here we use these two models to study the alloying effect on He by a local and small scale (about 100 atoms) change in the electronic structure.

Since the electronic structures of H and T, He and ^{3}He, are almost the same, it is reasonable to use H (He) as a replacement to simulate the electronic behavior of T (^{3}He) in metal tritides if ZPE effects were not included in the calculations. In fact, ZPE correction has less effect on the calculated results for TiT_2 than TiH_2 because the mass of T atom is three times that of H atom. For example, the calculated equilibrium lattice constant without ZPE correction was 4.29 Å for TiH_2 given by Yang et al. [26], about 0.15 Å less than the corresponding experimental value (4.44 Å); however, that given by us for TiT_2 (4.32 Å) is only 0.08 Å less than the experimental value (4.40 Å), about 2% less than the corresponding experimental one, which is an acceptable discrepancy in LDA approach.

In the calculations, the atomic geometric relaxation was performed by calculating the binding energy of a cluster of different fixed lattice constant in the limit of keeping the symmetry of the cluster. To examine the stability of He at the tetrahedral site(s) and at the octahedral site(s), respectively, the binding energies $E^{\mathrm{He}}_{\mathrm{Ti4}}$ and $E^{\mathrm{He}}_{\mathrm{Ti8}}$ are calculated. The following calculations of the alloying effects on the migration ability of He or on the stability of the clusters are performed in the same way with only one exception that the atom marked M (originally M = Ti for unalloyed condition) in both clusters in Fig. 1(a) and 2 is in turn substituted by alloying elements M (M = Sc, V, Cr, Mn, Fe, Co, Ni, Cu, Zn, Y, Zr, Nb, Mo, Tc, Ru, Rh, Pd, Ag, Cd). In the calculations, the binding energies for these models with M are notated as $E^{\mathrm{He}}_{\mathrm{M4}}$ and $E^{\mathrm{He}}_{\mathrm{M8}}$.

The atomic bond order $\mathrm{BO}_{\mathrm{A-B}}$ between atoms A and B, which can be evaluated by the Mulliken population analysis [31], is defined as

$$\mathrm{BO}_{\mathrm{A-B}} = \sum_{l} n_l \sum_{m' \in B} \sum_{m \in A} \alpha_{lm} \alpha_{lm'} S_{mm'}, \tag{2}$$

where α_{lm} and $\alpha_{lm'}$ are the coefficients of the atomic orbital m and m' in the molecular orbital l, $S_{mm'}$ is an overlap matrix element between two atomic orbitals m and m', n_l is the occupied charge of the molecular orbital l. BO_{A-B} is used to evaluate the strength of the covalent bond between atoms A and B.

Similarly, the orbital bond order (OBO) between two orbitals m and m' is defined as

$$OBO_{m-m'} = \sum_l n_l \alpha_{lm} \alpha_{lm'} S_{mm'}. \quad (3)$$

The crystal orbital overlap population (COOP), which presents the bonding character, can be used to measure the overlap degree of different atomic orbitals in an energy region [32,33]. The interpretation of COOP curve is straightforward: if the value of a curve over certain energy ranges is positive, the orbitals of the two atoms in question are in bonding state, otherwise they are in anti-bonding state.

3. Results and analyses

3.1. Migration ability of He in TiT_2

First of all, the equilibrium lattice constants of these two models are searched, and the results are plotted in Fig. 3(a). Both models give the same equilibrium constant of 4.32 Å, indicating that the sizes of these two models are acceptable. Fig. 3(b) and (c) present the dependence of binding energy on lattice constant for the two models with He at either the tetrahedral site (E^{He}_{Ti4}) or the octahedral site (E^{He}_{Ti8}). We note that the replacement of one T atom by one He atom makes the symmetry of model 1 change from Oh to C3, and in this case no equilibrium lattice constant is found as shown in Fig. 3(b), which indicates this state of one He alone is unstable; while for the configuration of replacing eight T atom by eight He atom in model 2 with Oh symmetry kept, there is an equilibrium lattice constant as shown in Fig. 3(c), indicating it is a stable configuration. The comparison between Fig. 3(b) and (c) seems to tell us that He would prefer to congregate in the form of a bubble, which is consistent with experiment.

In Fig. 3(b) for model 1, E^{He}_{Ti4} is larger than E^{He}_{Ti8} : $E^{He}_{Ti4} - E^{He}_{Ti8} = 0.48$–$0.58$ eV, indicating that He prefers the tetrahedral interstitial site to the octahedral interstitial site. This is quite consistent with the view that in early aging stage He atoms are still trapped interstitially in metal tritides [2,4]. On the other hand, in Fig. 3(c) for model 2, the situation is different: E^{He}_{Ti4} is less than E^{He}_{Ti8} and the absolute energy difference, $|E^{He}_{Ti4} - E^{He}_{Ti8}| = 4.89$–$6.67$ eV,

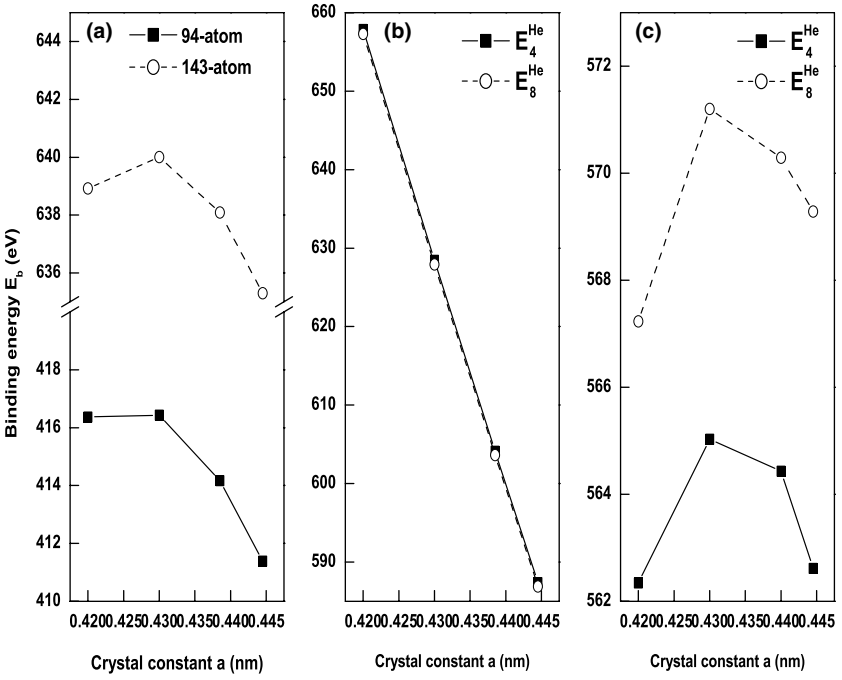

Fig. 3. Binding energy E_b as a function of lattice constant a with M = Ti. (a) symmetry = Oh with T at tetrahedral site for 94- and 143-atom clusters, (b) symmetry = C3 with He for 94-atom cluster, (c) symmetry = Oh with He for143-atom cluster.

and the average per He atom is 0.61–0.83 eV, about 0.13–0.25 eV larger than that in model 1. These show that as He concentration increases in the way as model 2, the preferring sites of He are no longer the tetrahedral sites but instead the octahedral sites, in agreement with the experimental fact reported by Weaver and Camp [4] that He atoms in Ti tritide aging for 1 yr will occupy the octahedral sites; and the tendency is so strong that the 8 He atoms will push not only with each other but also those atoms around them, resulting in a swelling effect in ditritides, which can be seen from the change in equilibrium lattice constant from 4.32 Å in Fig. 3(a) to 4.34 Å in Fig. 3(c), consistent with the molecular dynamics simulation of He bubble growth in metals [34]. From the viewpoint of either Weaver and Camp [4] or Wilson et al. [5], this should be attributed to the strong repulsive interaction between He and M atoms, which will be detailed further in Section 3.3.

From the above results, we may conclude that to prolong the service life of TiT_2, a good alloying element introduced should satisfy two requirements: (1) it is able to decrease the migration ability of He to prevent or reduce the occurrence of large He bubbles; (2) it has small repulsive interaction with He to increase the stability of TiT_2 system. Simply, a good alloying element should be a stronger trapper for its neighbor He atom(s) than Ti.

3.2. Alloying effect on the stability of He in TiT_2

Before going into this section, we need to examine further the influence of the boundary conditions in the surface region of the cluster on our DV-X_α calculations. For this purpose, an enlarged 126-atom cluster for model 1 is adopted, as shown in Fig. 1(b), whose difference from Fig. 1(a) is to add 32 T atoms around model 1 in Fig. 1(a). After the atom Ti at M site has been in turn substituted by alloying element M (M = Sc, V, Cr, Mn, Fe, Co, Ni, Cu, Zn, Y, Zr, Nb, Mo, Tc, Ru, Rh, Pd, Ag, Cd) in Fig. 1(a) and 1(b), the binding energies for He at either the tetrahedral site (E^{He}_{M4}) or the octahedral site (E^{He}_{M8}) are calculated at the lattice constant of 4.30 Å. Fig. 4(a) and (b) shows the dependence of $E^{He}_{M4(8)} - E^{He}_{Ti4}$ on the alloying element M for the 94-atom and the 126-atom cluster, respectively. It can be seen that these two curves are quite similar to each other, which indicates that the absence of 32 T atoms on the surface of the 126-atom cluster has little influence on the computed results, so that the 94-atom cluster is sufficiently large to simulate the He behavior in alloyed TiT_2, that is, the conclusions drawn from the results of the 94-atom cluster in Section 3.1 are reliable.

The $E^{He}_{M4(8)} - E^{He}_{Ti4}$ versus alloying element curves at given lattice constants are plotted in Fig. 5(a)–(d) for model 1 as shown in Fig. 1(a) and in

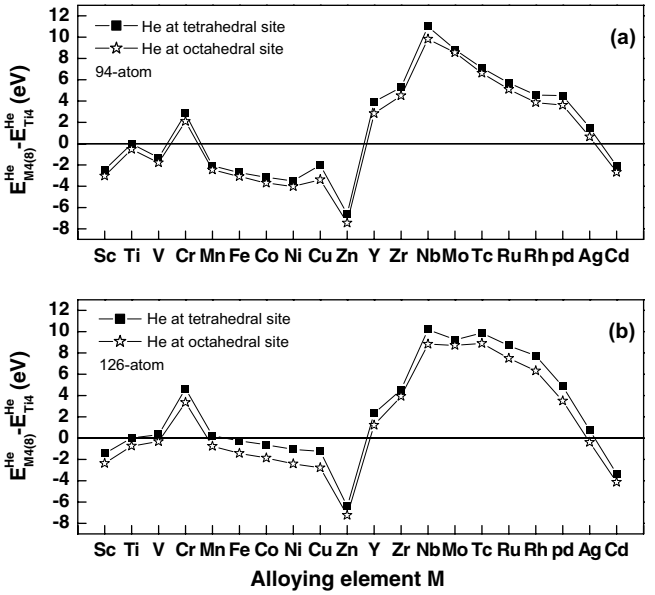

Fig. 4. The binding energy difference $E^{He}_{M4(8)} - E^{He}_{Ti4}$ as a function of alloying element M for different size of cluster with low He concentration. (a) 94-atom cluster, (b) 126-atom cluster. The lattice constant a used in both clusters is 4.30 Å. The solid square represents $E^{He}_{M4} - E^{He}_{Ti4}$ while the hollow star represents $E^{He}_{M8} - E^{He}_{Ti4}$.

Fig. 5(e) and (f) for model 2 as shown in Fig. 2. We can find that the shape of theses curves in Fig. 5(a)–(d) (or in Fig. 5(e) and (f)) does seldom change, suggesting that the alloying effect is not affected by the He-induced lattice change but dominated by the electronic structures of He-doped TiT_2 with the alloying elements.

The M-induced effect on the cluster stability could be measured by $E^{He}_{M4} - E^{He}_{Ti4}$, while its effect on the migration ability of He from tetrahedral sites to octahedral sites could be measured by $E^{He}_{M4} - E^{He}_{M8}$. Fig. 5(a)–(d) for model 1 show the values of $E^{He}_{M4} - E^{He}_{M8}$ to be between 0.24 and 1.38 eV, indicating to what extent a He atom prefers a tetrahedral site to an octahedral site for different alloying element M. In contrast with Fig. 5(a)–(d), the values of $E^{He}_{M4} - E^{He}_{M8}$ are between −0.36 and −13.90 eV in Fig. 5(e) and (f) for model 2. The negative values imply that despite different alloying elements introduced, He atoms will eventually prefer the octahedral sites to the tetrahedral sites as the He concentration increases.

Since the purpose of introducing alloying elements is to prevent or delay the formation of large He bubbles, He atoms in the tritide being trapped deeper at their born tetrahedral interstitial sites are desired. It is quite natural to realize that the alloying elements with larger positive values of $E^{He}_{M4} - E^{He}_{Ti4}$ and $E^{He}_{M4} - E^{He}_{M8}$ are better. To quantitatively measure the priority of one alloying element over others in the sense of making He be trapped at the tetrahedral site, two variables, K_L and K_H are simply defined, K_L is for model 1 with low He concentration and K_H is for model 2 with high He concentration. It is easily known from above description that K_L is proportional to the product of $E^{He}_{M4} - E^{He}_{Ti4}$ multiplied by $E^{He}_{M4} - E^{He}_{M8}$, while K_H is proportional to the quotient of $E^{He}_{M4} - E^{He}_{Ti4}$ divided by $|E^{He}_{M4} - E^{He}_{M8}|$ because of the negative value of $E^{He}_{M4} - E^{He}_{M8}$. In the concrete, the scaled K_L and K_H as a function of alloying element M are defined as follows:

$$K_L(M) = \frac{E^{He}_{M4} - E^{He}_{Ti4}}{\left(E^{He}_{M4} - E^{He}_{Ti4}\right)_{max}} \cdot \frac{E^{He}_{M4} - E^{He}_{M8}}{\left(E^{He}_{M4} - E^{He}_{M8}\right)_{max}}, \quad (4)$$

$$K_H(M) = \frac{E^{He}_{M4} - E^{He}_{Ti4}}{\left|E^{He}_{M4} - E^{He}_{Ti4}\right|_{max}} \Bigg/ \frac{\left|E^{He}_{M4} - E^{He}_{M8}\right|}{\left|E^{He}_{M4} - E^{He}_{M8}\right|_{max}}, \quad (5)$$

where $\left(E^{He}_{M4} - E^{He}_{Ti4}\right)_{max}$, $\left(E^{He}_{M4} - E^{He}_{M8}\right)_{max}$ and $\left|E^{He}_{M4} - E^{He}_{M8}\right|_{max}$ are, respectively, the maximums of $E^{He}_{M4} - E^{He}_{Ti4}$, $E^{He}_{M4} - E^{He}_{M8}$ and $\left|E^{He}_{M4} - E^{He}_{M8}\right|$ for all M. The physical meaning of K_L and K_H is that the larger they are, the more beneficial to trapping He

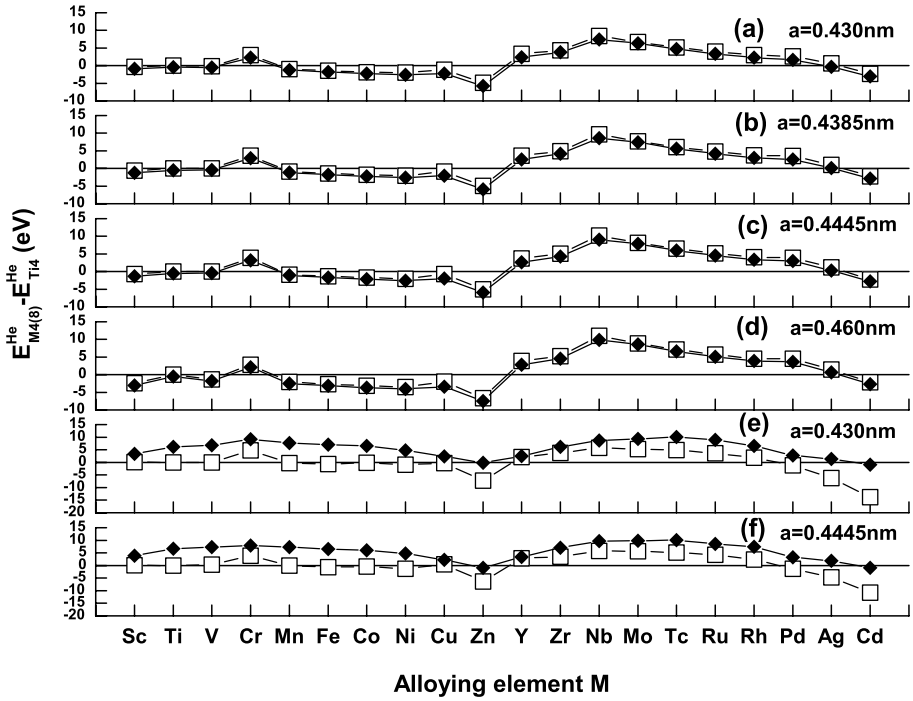

Fig. 5. The binding energy difference $E^{He}_{M4(8)} - E^{He}_{Ti4}$ as a function of alloying element M at different lattice constant a. (a) In model 1, (b) in model 2. The hollow square represents $E^{He}_{M4} - E^{He}_{Ti4}$ while the solid diamond represents $E^{He}_{M8} - E^{He}_{Ti4}$.

atoms at the tetrahedral sites, or the more difficult for He to leave these sites, with alloying.

According to the average values of K_L and K_H plotted, respectively, in Fig. 6(a) and (b) for different lattice constants, the priority of alloying elements are ranked in descending order as: Nb > Y > Zr > Pd > Ru > Tc > Rh > Cr > Mo > Ag > Ti > V > Mn > Sc > Fe > Co > Ni > Cu > Cd > Zn for model 1 and Y > Nb > Mo > Zr > Cr > Tc > Ru > Rh > Cu > Sc > V > Ti > Mn > Co > Fe > Ni > Pd > Ag > Cd > Zn for model 2. It can be concluded from the above results that compared with Ti, most of the 4d transition metal elements have beneficial effects on trapping He at the tetrahedral sites while most of the 3d transition metal elements have detrimental effects, and among them, Y, Nb, Mo and Zr are surprisingly beneficial while Zn, Cd extremely detrimental.

3.3. Alloying effect on chemical bonding between He and alloying element M

3.3.1. In model 1

The BO and OBO, of which the BO is mainly composed, are shown as a function of alloying element M in Fig. 7(a) and (b) for He at the tetrahedral site and at the octahedral site, respectively. The values of $BO_{M–He}$ in Fig. 7(a) are mostly positive and the magnitude for a given M is at least 2 orders larger than the corresponding one in Fig. 7(b). This comparison indicates that the interaction between M and He at the tetrahedral site is much stronger than that at the octahedral site and, except for M = Ag, Cd, almost all of M are in a binding state with He although the bonding strength (the value of $BO_{M–He}$) is quite different from each other.

In Fig. 7(a), $OBO_{Mnd–He}$ ($n = 3$ for 3d transition metal and $n = 4$ for 4d transition metal) has quite a similar value and trend to $BO_{M–He}$, so it should be a decisive component of $BO_{M–He}$. Comparing Fig. 7(a) with Fig. 6(a), we find that the trend of the $BO_{M–He}$ is similar to that of K_L. Therefore, as a decisive component of $BO_{M–He}$, the positive (bonding) value of $OBO_{Mnd–He}$, may be used to evaluate the stability of He at the tetrahedral site. In one word, M's *n*d orbital electrons play an important role in the chemical bonding and thus in its alloying effect on the stability of He in titanium ditritide.

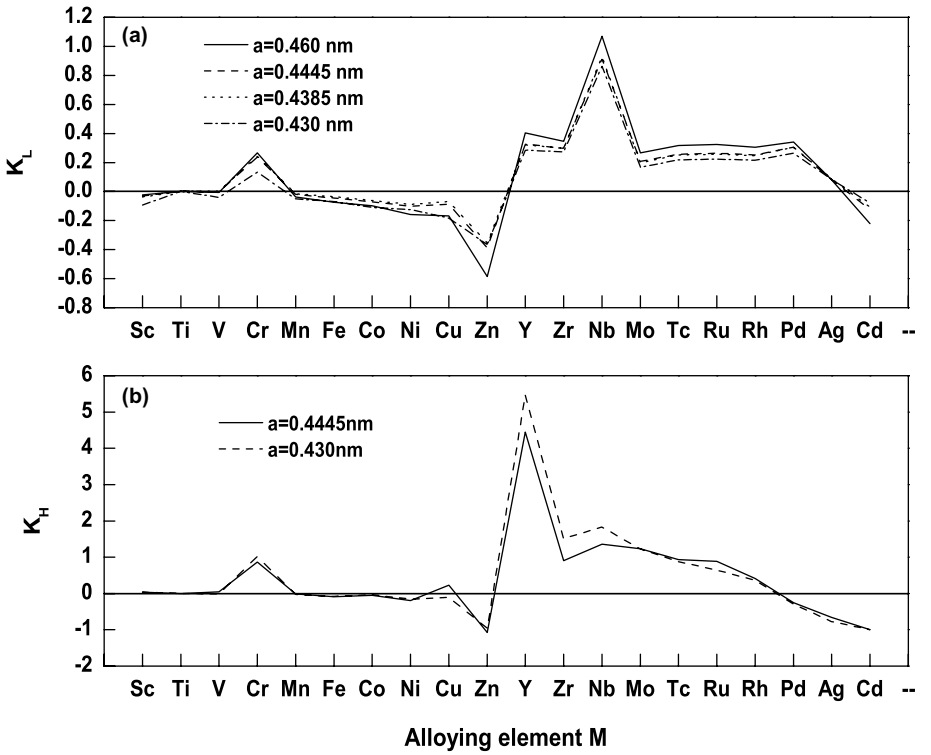

Fig. 6. (a) K_L for model 1, (b) K_H for model 2, as a function of alloying element M at different lattice constant *a*.

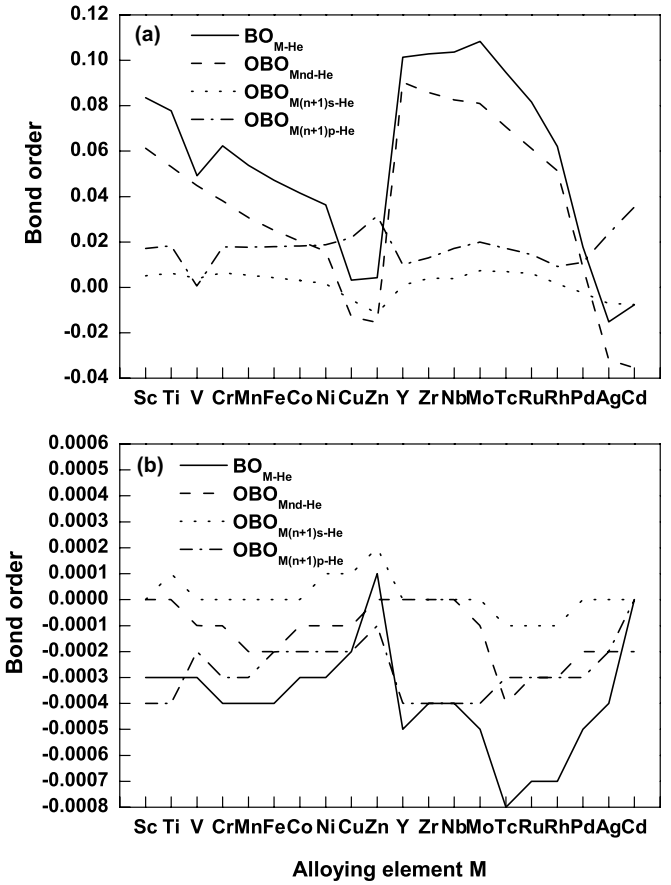

Fig. 7. Bond order between alloying element M and He as a function of M in model 1. (a) when He at the tetrahedral site, (b) when He at the octahedral site.

3.3.2. In model 2

With the same reason as above, more attention is paid to Fig. 8(a), in which the magnitude of $BO_{M–He}$ is at least 2 orders larger than the corresponding one in Fig. 8(b). In contrast to those in Fig. 7(a), most values in Fig. 8(a) are negative, this indicates that as He in TiT_2 accumulates to a high concentration (He/Ti $\approx$ 14.55 at.%) in the way as shown in Fig. 2, almost all interactions of the alloying element M with He atoms at the first-neighbor tetrahedral sites, except for Y and Zr, are repulsively anti-bonding, which would lead to the swelling of the lattice.

In Fig. 8(a), $OBO_{M(n+1)s–He}$, not $OBO_{Mnd–He}$ as in model 1, becomes the decisive component of $BO_{M–He}$. This may be attributed to the different symmetry from model 1. In model 1, there is only one He atom in the nearest neighbor of the alloying element M and it is in the direction of M's d_{xy} orbital, therefore the interaction between He's 1s and M's *n*d orbitals is quite strong. While in model 2 there are 8 He atoms around only one alloying element M, such a spherical distribution of He atoms may be advantageous to the interaction between the spherical He's 1s and M's $(n + 1)$s orbitals. We also find in this case that the variation of $BO_{M–He}$ (or $OBO_{M(n+1)s–He}$) with M is similar in trend to that of K_H in Fig. 6(b), indicating that the repulsive anti-bonding interaction between M and He ($BO_{M–He}$ or $OBO_{M(n+1)s–He}$) at the tetrahedral sites is mainly responsible for the priority of alloying element M.

An image of the structure evolution in TiT_2 during T decay can be deduced from the results in Sections 3.3.1 and 3.3.2: in the early aging time He concentration is low and He atoms randomly and solely distributed in TiT_2, the bonding interaction $BO_{M–He}$ (mainly $OBO_{Mnd–He}$) makes these He atoms be trapped at the tetrahedral sites; however, He atoms will accumulate as time goes by, when the He bubble-like configure as shown in model 2

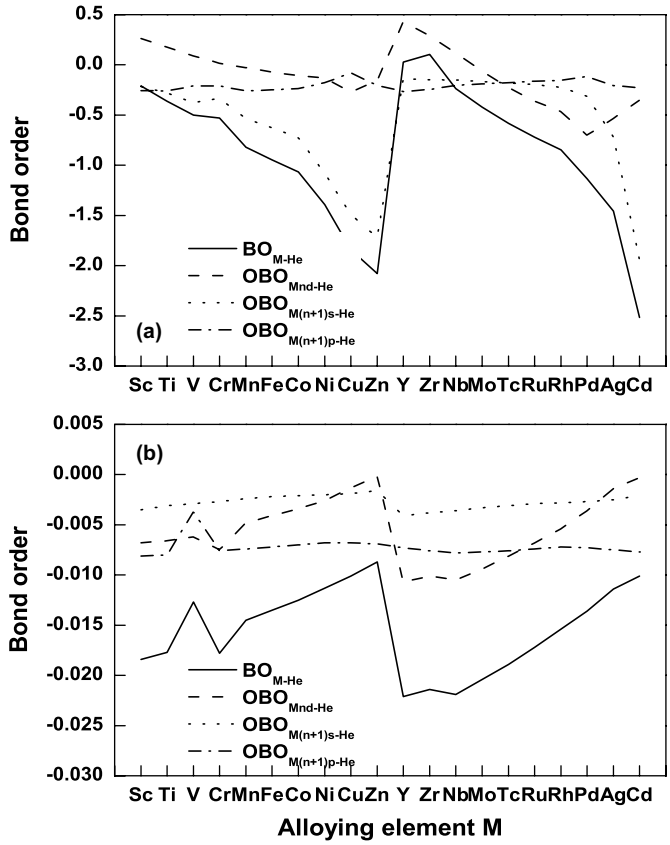

Fig. 8. Bond order between alloying element M and He as a function of M in model 2. (a) when He at the tetrahedral site, (b) when He at the octahedral site.

occurs, BO_{M-He} will become repulsive anti-bonding and will make those He atoms in close vicinity to M be pushed from the tetrahedral sites into the octahedral sites, leading to a swelled lattice of TiT_2. In other words, a good alloying element M should work in different way at different aging times: in the early stage, it has to try for trapping He deeply at the tetrahedral site to prevent the formation of He bubbles; while in the older stage, it has to reduce the repulsive interaction with He atoms to delay the outburst of large He bubbles.

3.4. Density of states (DOS) and COOP analysis

To explore further why the alloying effects of these transition metal elements are different in the two models, the DOS and COOP of Nb and Y with the beneficial effects and Zn and Cd with the detrimental effects, for example, are calculated and compared.

3.4.1. In model 1

The partial DOS (PDOS) curves of M (M = Nb, Ti, Zn) and He and their COOP in TiT_2 are plotted in Fig. 9, where Fermi level (E_F) is set at zero as a reference. There are two 1s PDOS bands for He atom, one stronger 1sσ band appears in a low energy region approximately −15.1 eV in Fig. 9(a), (c) and (e) for He atom at the tetrahedral site while −13.9 eV in Fig. 9(b), (d) and (f) for He atom at the octahedral site, the other weaker 1sσ* band is in a energy region closer to E_F (above −10.0 eV) as magnified in the insets in the corresponding figures. The PDOS of Nb (Ti), which is the sum of Nb (Ti)'s nd, $(n+1)$s and $(n+1)$p PDOS, is unchanged regardless of He at the tetrahedral site or at the octahedral site, however, the value of He 1sσ* band when He at the octahedral site is much larger than that when He at the tetrahedral site, leading to an anti-bonding COOP as shown in Fig. 9(b′) and (d′) but a bonding COOP in Fig. 9(a′) and (c′). Such bonding character of He with Nb (Ti) makes He prefer to be trapped at

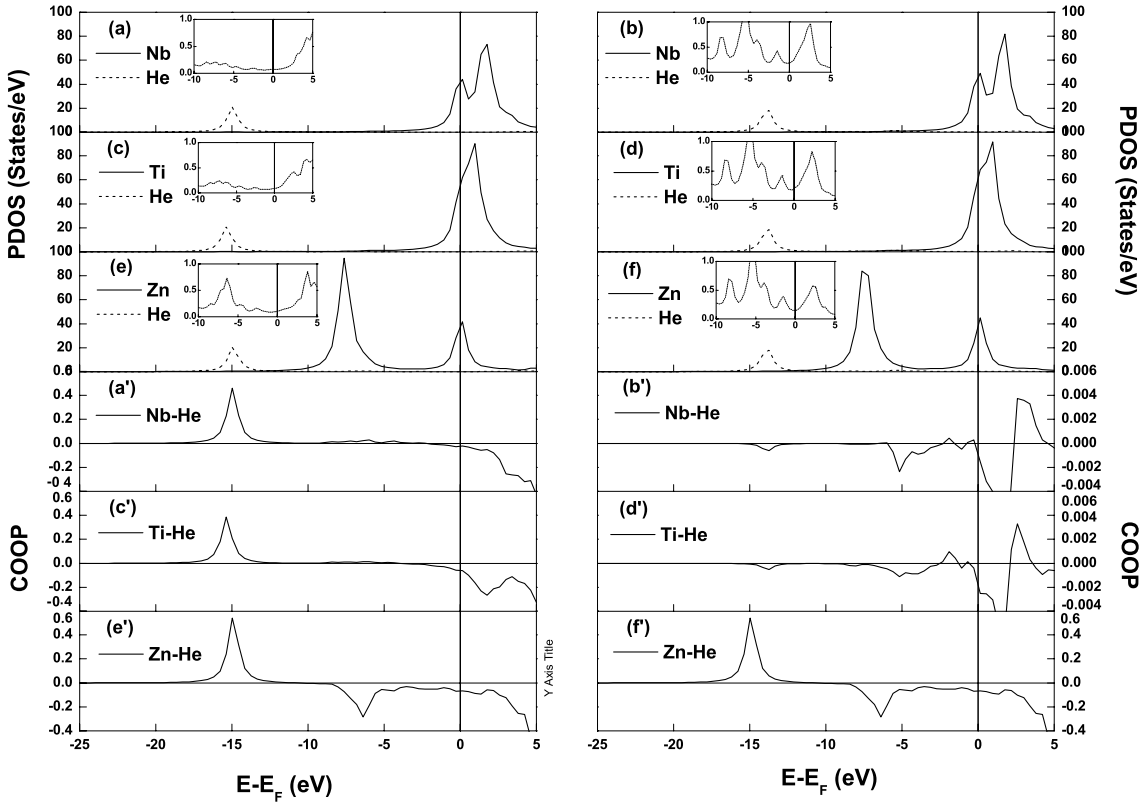

Fig. 9. PDOS of He and alloying element M (M = Nb, Ti, Zn) together with COOP between them in model 1 at the lattice constant $a = 0.430$ nm. The left-column curves ((a), (c), (e), (a′), (c′) and (e′)) are for He at the tetrahedral site, the right-column curves ((b), (d), (f), (b′), (d′) and (f′)) are for He at the octahedral site.

the tetrahedral site. For Zn, the case is somewhat different. Firstly, the He 1sσ* band becomes stronger when He at the tetrahedral site, comparable to that when He at the octahedral site. Secondly, the almost same and strong Zn PDOS peaks overlap with the He 1sσ* band at about −8 eV for both sites. As a result, the COOP for He at the tetrahedral site (Fig. 9(e′)) is similar to that for He at the octahedral site (Fig. 9(f′)), which explains why the introduction of Zn into TiT_2 is not beneficial to trapping He at its born tetrahedral site.

Fig. 9 shows clearly that in the case of low He concentration, the alloying effect of M on trapping He at the tetrahedral site (the stability of He) is closely related to the bonding interaction between M and He.

3.4.2. In model 2

In model 2 with He bubble-like configuration, the stronger He 1sσ band appears in a low energy region approximately −22.3 eV in Fig. 10(a), (c) and (e) for He atoms at the tetrahedral sites but −17.6 eV in Fig. 10(b), (d) and (f) for He atoms at the octahedral sites, the weaker He 1sσ* band magnified in the insets in Fig. 10 is in a energy region closer to E_F (above −15.0 eV). Different from Fig. 9, the PDOS of Y (Ti or Cd) overlaps more strongly with the He 1sσ* band. Such a strong overlap results in the increase in anti-bonding interaction between Y (Ti or Cd) and He as shown in Fig. 10(a′)–(f′). However, the COOP between Y and He for He at the tetrahedral sites still presents a binding interaction between them but an anti-bonding one when He at the octahedral sites. In contrast with the case of Y, the COOP between Cd (Ti) and He for at both sites are in anti-bonding state, this explains further why Y is still a beneficial alloying element to stabilizing He at its born site even in the extreme case of He bubble-like but Cd (Ti) is not. Though M has positive interaction with He at tetrahedral sites but negative one with those at octahedral sites, there are much stronger negative interactions among He atoms at tetrahedral sites, which will overwhelm the attractive interaction

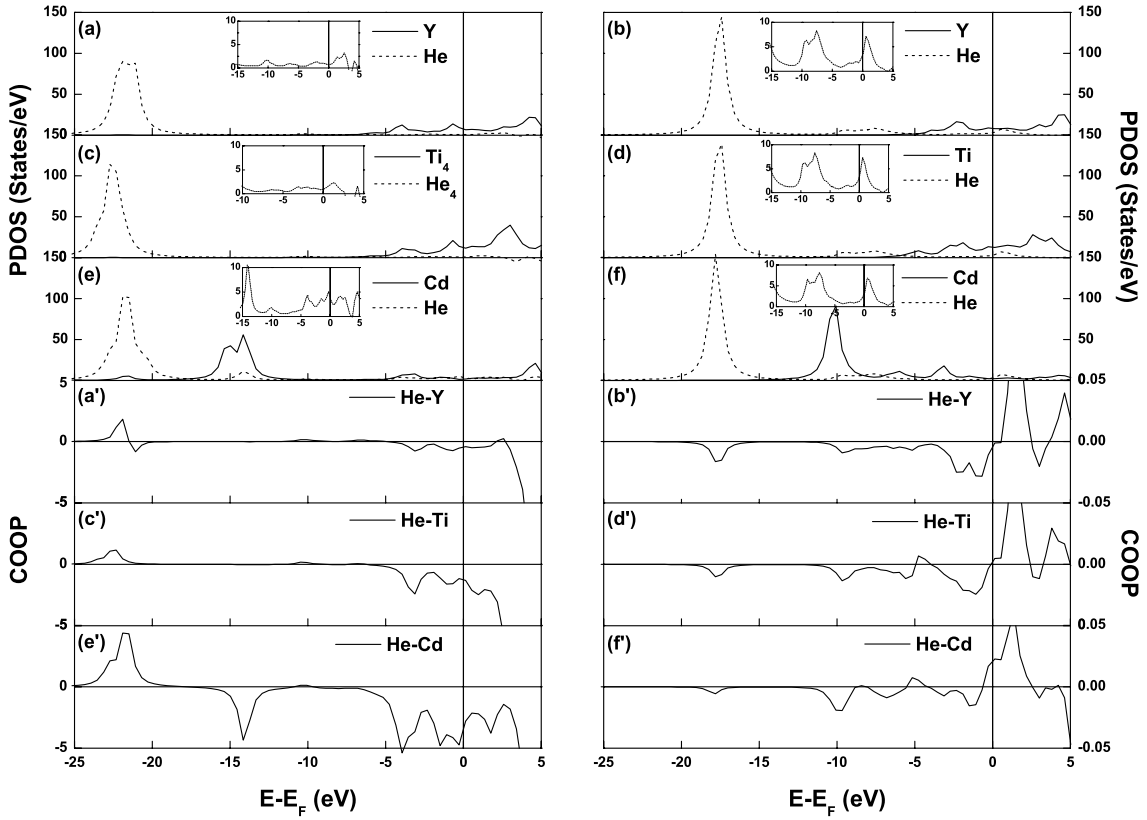

Fig. 10. PDOS of He and alloying element M (M = Y, Ti, Cd) together with COOP between them in model 2 at the lattice constant $a = 0.430$ nm. The curves here have the same meaning as those in Fig. 9.

between M and He, resulting in the He atoms' preference of octahedral sites.

3.5. Experiment evidence: analysis of the PAS results

To convince the above computed results of alloying effect we have performed a series of PAS measurements [35] for Ti, TiMoYAl and TiZrYAl films about 1 μm, implanted at 60 KeV with He fluence of $1.0 \times 10^{17}\,\mathrm{cm}^{-2}$ at room temperature and annealed 1hr isochronally at 200 °C, 400 °C, 700 °C and 850 °C.

The maximum difference ΔS of the S parameter of these samples minus the S value of the defect-free reference sample treated by He-implanting and then annealing is used to roughly estimate the positron annihilation with electrons with low momentum: this difference is related to positrons trapped in open volume defects [35–37]. As was pointed out by Brusa et al. [37], the ΔS is closely related to those vacancies involved in the He clustering process by decreasing the energy necessary to accommodate successive He atoms. In our experiments of these samples implanted, aged for one and two months and annealed at 200 °C, the ΔS value is ~0.04 for Ti, about 2 times larger than ~0.02 for TiMoYAl and TiZrYAl and the full-width half-maximum (FWHM) of the curve of ΔS vs. positron implantation energy E is about 7.5 KeV for Ti but 9.0 KeV for TiMoYAl and TiZrYAl, indicating that the vacancy agglomerate in Ti is much higher than in TiMoYAl and TiZrYAl and those vacancies are distributed in a more narrow range for the former than for the latter. In TiMoYAl and TiZrYAl, the reason why such clustering tendency is highly reduced, comparing with that in Ti film, may be that a majority of He atoms are trapped at interstitial sites by alloying as mentioned in Section 3.2, so that a majority of vacancies can form vacancy complexes only with these trapped He atoms and be distributed in a broader range, making those vacancies less efficiently be detected by PAS due to the He-induced passivation.

The above analysis of PAS experimental results support our prediction that Y, Mo, and Zr are more

beneficial than Ti to trapping He atom in an alloyed Ti-based alloy. The further analysis of PAS measurements of the annealed samples at 400 °C, 700 °C and 850 °C will be given in a separate paper [38].

4. Summary

Two models are proposed to study the alloying effects of 3d and 4d transition metals on the migration ability of He in TiT_2 with a low and a high He concentration, respectively. It is found that He prefers to stay trapped at the tetrahedral site for the low He concentration (He/Ti $\approx$ 2.63 at.%), but at the octahedral site for the high He concentration (He/Ti $\approx$ 14.55 at.%). Such a site preference of He can be modified by alloying of TiT_2: for TiT_2 with the low He concentration, Nb, Y, Zr, Pd, Ru, Tc, Rh, Cr, Mo and Ag can be used to trap He more deeply at the tetrahedral site than Ti; for TiT_2 with the high He concentration, compared with Ti, the introduction of Y, Nb, Mo, Zr, Cr, Tc, Ru, Rh and Cu can reduce the repulsive interaction between M and He atoms, which will consequently reduce the tritide fragility caused by the volume expansion and outburst of He bubbles. The analysis of the electronic structure of the aged TiT_2 shows that the stability of He at its born tetrahedral site depends essentially on the interaction between the alloying element M and He and thus BO_{M-He} for He at the tetrahedral site could be used as a measurement of the stability of He and of the alloying effect of M. The results of our PAS experiments verify to some extent our conclusion about good alloying element.

Acknowledgments

The authors thank Dr J.Y. Wang and Dr Y.C. Zhou for their help on calculation. This work was supported by National Natural Science Fund of China (Grant No. 50271071).

References

[1] R. Lässer, J. Less-Common Met. 131 (1987) 263.
[2] W.J. Camp, J. Vac. Sci. Technol. 14 (1977) 514.
[3] R.P. Gupta, M. Gupta, Phys. Rev. B 66 (2002) 014105.
[4] H.T. Weaver, W.J. Camp, Phys. Rev. B 12 (1975) 3054.
[5] W.D. Wilson, C.L. Bisson, M.I. Baskes, Phys. Rev. B 24 (1981) 5616.
[6] H. Trinkaus, B.N. Singh, J. Nucl. Mater. 323 (2003) 229.
[7] T. Schober, H. Trinkaus, Philos. Mag. A 65 (1992) 1235.
[8] M.P. Shaw, B. Ralph, W. M Stobbs, J. Nucl. Mater. 115 (1983) 1.
[9] T. Schober, R. Lässer, J. Nucl. Mater. 120 (1984) 137.
[10] R.C. Bowman, A. Attalla, Phys. Rev. B 16 (1977) 1828.
[11] W.D. Wilson, M.I. Baskes, C.L. Bisson, Phys. Rev. B 13 (1976) 2470.
[12] L.K. Mansur, E.H. Lee, P.J. Maziasz, A.P. Rowcliffe, J. Nucl. Mater. 141–143 (1986) 633.
[13] P.J. Goodhew, S.K. Tyler, M.B. Waldron, J. Nucl. Mater. 103&104 (1981) 1151.
[14] T. Schober, K. Farrell, J. Nucl. Mater. 168 (1989) 171.
[15] R.L. Whetten, D.M. Cox, D.J. Trevor, A. Kaldor, Phys. Rev. Lett. 54 (1985) 1494.
[16] P. Jena, B.K. Rao, S.N. Khanna, J. Less-Common Met. 172–174 (1991) 387.
[17] N. Watari, S. Ohnishi, Y. Ishii, J. Phys.: Condens. Matter 12 (2000) 6799.
[18] C.Y. Yang, K.H. Johnson, D.R. Salahub, J. Kaspar, R.P. Messmer, Phys. Rev. B 24 (1981) 5673.
[19] Y. Takahashi, H. Yukawa, M. Morinaga, J. Alloys Compd. 242 (1996) 98.
[20] M. Gupta, E. Belin, L. Schlapbach, J. Less-Common Met. 103 (1984) 389.
[21] H. Yukawa, M. Morinaga, Y. Takahashi, J. Alloys Compd. 253&254 (1997) 322.
[22] T. Matsumura, H. Yukawa, M. Morinaga, J. Alloys Compd. 279 (1998) 192.
[23] K. Nakatsuka, M. Yoshino, H. Yukawa, M. Morinaga, J. Alloys Compd. 293–295 (1999) 222.
[24] T. Matsumura, H. Yukawa, M. Morinaga, J. Alloys Compd. 284 (1999) 82.
[25] H. Yukawa, T. Matsumura, M. Morinaga, J. Alloys Compd. 293–295 (1999) 227.
[26] R. Yang, Y.M. Wang, Y. Zhao, L.B. Wang, H.Q. Ye, C.Y. Wang, Acta Mater. 50 (2002) 109.
[27] D.E. Ellis, G.S. Painter, Phys. Rev. B 2 (1970) 2887.
[28] U. Von Barth, L. Hedin, J. Phys. C 5 (1972) 1629.
[29] R.O. Jones, O. Gunnarson, Rev. Mod. Phys. 61 (1989) 689.
[30] C. Wolverton, V. Ozoliņš, M. Asta, Phys. Rev. B 69 (2004) 144109.
[31] R.S. Mulliken, J. Chem. Phys. 23 (1955) 1833, 1841, 2338, 2343.
[32] R. Hughbanks, R. Hoffmann, J. Am. Chem. Soc. 105 (1983) 3528.
[33] S.D. Wijeyesekera, R. Hoffmann, Organometallics 3 (1984) 949.
[34] S.M. Foiles, J.J. Hoyt, Sandia Report, 2001, SAND2001-0661.
[35] A. Dupasquier, A.P. Mills Jr., Positron Spectroscopy of Solids, North-Holland, Amsterdam, 1995.
[36] P. Asoka-Kumar, K.G. Lynn, D.O. Welch, J. Appl. Phys. 76 (1994) 4935.
[37] R.S. Brusa, G.P. Karwasz, N. Tiengo, A. Zecca, F. Corni, R. Tonini, G. Ottaviani, Phys. Rev. B 61 (2000) 10154.
[38] H. Zheng, S. Liu, L.B. Wang, unpublished.